Automated quantification of floating wood pieces in rivers from video monitoring: a new software tool and validation.

Hossein Ghaffarian[1, *,] Pierre Lemaire[1,2], Zhang Zhi[1], Laure Tougne[2], Bruce MacVicar[3], and Hervé Piégay[1]

[1]Univ. Lyon, UMR 5600, Environnement-Ville-Société CNRS, F-69362 Lyon, France
[2]Univ. Lyon, UMR 5205, Laboratoire d'InfoRmatique en Image et Systèmes d'information CNRS, F-69676 Lyon, France
3Department of Civil and Environmental Engineering, Univ. Waterloo, Waterloo, Ontario, Canada

Correspondence to: Hossein Ghaffarian (hossein.ghaffarian@ens-lyon.fr)

Abstract

Wood is an essential component of rivers and plays a significant role in ecology and morphology. It can be also considered as a risk factor in rivers due to its influence on erosion and flooding. Quantifying and characterizing wood fluxes in rivers during floods would improve our understanding of the key processes but is hindered by technical challenges. Among various techniques for monitoring wood in rivers, streamside videography is a powerful approach to quantify different characteristics of wood in rivers, but past research has employed a manual approach that has many limitations. In this work, we introduce new software for the automatic detection of wood pieces in rivers. We apply different image analysis techniques such as static and dynamic masks, object tracking, and object characterization to minimize false positive and missed detections. To assess the software performance, results are compared with manual detections of wood from the same videos, which was a time-consuming process. Key parameters that affect detection are assessed including surface reflections, lighting conditions, flow discharge, wood position relative to the camera, and the length of wood pieces. Preliminary results had a 36% rate of false positive detection, primarily due to light reflection and water waves, but post-processing reduced this rate to 15%. The missed detection rate was 71% of piece numbers in the preliminary result, but post processing reduced this error to only 6.5% of piece numbers, and 13.5% of volume. The high precision of the software shows that it can be used to massively increase the quantity of wood flux data in rivers around the world, potentially in real time. The significant impact of post-processing indicates that it is necessary to train the software in various situations (location, timespan, weather conditions) to ensure reliable results. Manual wood detections and annotations for this work took more than one human-month of labor. In comparison, the presented software coupled with an appropriate post processing step performed the same task in real time (55 hr) on a standard desktop computer.

30   Keywords: River monitoring, Wood flux, Wood discharge, Large wood, Ground video imagery, Auto-
31   matic detection

1.   Introduction

33   Floating wood has a significant impact on river morphology (Gurnell et al., 2002; Gregory et al., 2003;
34   Wohl, 2013; Wohl and Scott, 2017). It is both a component of stream ecosystems and a source of risk for
35   human activities (Comiti et al., 2006; Badoux et al., 2014; Lucía et al., 2015). The deposition of wood at
36   given locations can cause a reduction of the cross-sectional area, which can both increase upstream water
37   levels (and the risk for neighboring communities), and laterally concentrate the flow downstream, which can
38   lead to damaged infrastructure (Lyn et al., 2003; Lagasse, 2010; Mao and Comiti, 2010; Badoux et al., 2014;
39   Ruiz-Villanueva et al., 2014; De Cicco et al., 2018; Mazzorana et al., 2018). Therefore, understanding and
40   monitoring the dynamics of wood within a river is fundamental to assess and mitigate risk. An important
41   body of work on this topic has grown over the last two decades, which has led to the development of many
42   monitoring techniques (Marcus et al., 2002; MacVicar et al., 2009a; MacVicar and Piégay, 2012; Benacchio
43   et al., 2015; Ravazzolo et al., 2015; Ruiz-Villanueva et al., 2018; Ghaffarian et al., 2020; Zhang et al., 2020)
44   and conceptual and quantitative models (Braudrick and Grant, 2000; Martin and Benda, 2001; Abbe and
45   Montgomery, 2003; Gregory et al., 2003; Seo and Nakamura, 2009; Seo et al., 2010). A recent review by
46   Ruiz-Villanueva et al. (2016), however, argues that the area remains in relative infancy compared to other
47   river processes such as the characterization of channel hydraulics and sediment transport. Many questions
48   remain open areas of inquiry including wood hydraulics, which is needed to understand wood recruitment,
49   movement and trapping, and wood budgeting, where better parametrization is needed to understand and
50   model the transfer of wood in watersheds at different scales.

51   In this domain, the quantification of wood mobility and wood fluxes in real rivers is a fundamental
52   limitation that constrains model development. Most early works were based on repeated field surveys (Keller
53   and Swanson, 1979; Lienkaemper and Swanson, 1987), with more recent efforts taking advantage of aerial
54   photos or satellite images (Marcus et al., 2003; Lejot et al., 2007; Lassettre et al., 2008; Senter and Pasternack,
55   2011; Boivin et al., 2017) to estimate wood delivery at larger time scales of 1 year up to several decades.
56   Others have monitored wood mobility once introduced by tracking wood movement in floods (Jacobson et
57   al., 1999; Haga et al., 2002; Warren and Kraft, 2008). Tracking technologies such as active and passive Radio
58   Frequency Identification transponders (MacVicar et al., 2009a; Schenk et al., 2014) or GPS emitters and

2

59   receivers (Ravazzolo et al., 2015) can improve the precision of this strategy. To better understand wood flux,

60   specific trapping structures such as reservoirs or hydropower dams can be used to sample the flux over time

61   interval windows (Moulin and Piégay, 2004; Seo et al., 2008; Turowski et al., 2013). Accumulations up-

62   stream of a retention structure can also be monitored where they trap most or all of the transported wood, as

63   was observed by Boivin *et al.* (2015), to quantify wood flux at the flood event or annual scale. All these

64   approaches allow the assessment of wood budget and the in-channel wood exchange between geographical

65   compartments within a given river reach and over a given period (Schenk et al., 2014; Boivin et al., 2015,

66   2017).

67   For finer scale information on the transport of wood during flood events, video recording of the water

68   surface is suitable for estimating instantaneous fluxes and size distributions of floating wood in transport

69   (Ghaffarian et al., 2020). Classic monitoring cameras installed on the river bank are cheap and relatively easy

70   to acquire, setup and maintain. As is seen in Table 1, a wide range of sampling rates and spatial/temporal

71   scales have been used to assess wood budgets in rivers. MacVicar and Piégay (2012) and Zhang et al., (2020)

72   (in review), for instance, monitored wood fluxes at 5 frames per second (fps) and a resolution of 640×480

73   up to 800×600 pixels. Boivin et al. (2017) used a similar camera and frame rate as MacVicar and Piégay

74   (2012) to compare periods of wood transport with and without the presence of ice. Senter et al. (2017) ana-

75   lyzed the complete daytime record of 39 days of videos recorded at 4 fps and a resolution of 2048×1536

76   pixels. Conceptually similar to the video technique, time-lapse imagery can be substituted when large rivers

77   where surface velocities are low enough and the field of view is large. Kramer and Wohl (2014); Kramer et

78   al. (2017) applied this technique in the Slave River (Canada) and recorded one image every 1 and 10 minutes.

79   Where possible, wood pieces within the field of view are then visually detected and measured using simple

80   software to measure the length and diameter of the wood to estimate wood flux (piece/s) or wood volume

81   (m^3/s) (MacVicar and Piégay, 2012; Senter et al., 2017). Critically for this approach, the time it takes for

82   the researchers to extract information about wood fluxes has limited the fraction of the time that can be

83   reasonably analyzed. Given the outdoor location for the camera, the image properties depend heavily on

84   lighting conditions (e.g. surface light reflections, low light, ice, poor resolution or surface waves) which may

85   also limit the accuracy of frequency and size information (Muste et al., 2008; MacVicar et al., 2009a). In

86   such situations, simpler metrics such as a count of wood pieces, a classification of wood transport intensity,

87   or even just a binary presence/absence may be used to characterize the wood flux (Boivin et al., 2017; Kramer

88   et al., 2017).

Earth **Surface**
Dynamics
Discussions

Open Access

EGU

Table 1

89   A fully automatic wood detection and characterization algorithm can greatly improve our ability to

90   exploit the vast amounts of data on wood transport that can be collected from streamside video cameras.

91   From a computer science perspective, however, automatic detection and characterization remain challenging

92   issues. In computer vision, detecting objects within videos typically consists of separating the foreground

93   (the object of interest) from the background (Roussillon et al., 2009; Cerutti et al., 2011, 2013). The basic

94   hypothesis is that the background is relatively static and covers a large part of the image, allowing it to be

95   matched between successive images. In the riverine environments, however, such an assumption is unrealistic

96   because the background shows a flowing river, which can have rapidly fluctuating properties (Ali and

97   Tougne, 2009). Floating objects are also partially submerged in water that has high suspended material con-

98   centrations during floods, making them only partially visible (*e.g.* a single piece of wood may be perceived

99   as multiple objects) (MacVicar et al., 2009b). Detecting such an object in motion within a dynamic back-

100   ground is an area of active research (Ali et al., 2012, 2014; Lemaire et al., 2014; Piégay et al., 2014; Be-

101   nacchio et al., 2017). Accurate object detection typically relies on the assumption that objects of a single

102   class (e.g. faces, bicycles, animals, etc.) have a distinctive aspect or set of features that can be used to distin-

103   guish between types of objects. With the help of a representative dataset, machine learning algorithms aim

104   at defining the most salient visual characteristics of the class of interest (Lemaire et al., 2014; Viola and

105   Jones, 2006). When the objects have a wide intra-class aspect range, a large amount of data can compensate

106   by allowing the application of deep learning algorithms (Gordo et al., 2016; Liu et al., 2020). To our

107   knowledge, such a database is not available in the case of floating wood.

108   The camera installed on the Ain River in France has been operating more or less continuously for over

109   10 years and vast improvements in data storage mean that this data can be saved indefinitely (Zhang et al.,

110   2020). The ability to process this image database to extract the wood fluxes allows us to integrate this infor-

111   mation over floods, seasons and years, which would allow us to significantly advance our understanding of

112   the variability within and between floods over a long time period. An unsupervised method to identify float-

113   ing wood in these videos by applying intensity, gradient and temporal masks was developed by Ali and

114   Tougne (2009) and Ali *et al.* (2011). In this model, the objects were tracked through the frame to ensure that

115   they followed the direction of flow. An analysis of about 35 minutes of the video showed that approximately

116   90% of the wood pieces was detected (*i.e.* about 10% of detection were missed), which confirmed the poten-

117   tial utility of this approach. An additional set of false detection related to surface wave conditions amounted

118   to approximately 15% of the total detection. However, the developed algorithm was not always stable and

119   was found to perform poorly when applied to a larger data set.

120   The objectives of the presented work are to describe and validate a new algorithm and computer inter-
121   face for quantifying floating wood pieces in rivers. First, the algorithm procedure is introduced to show how
122   wood pieces are detected and characterized. Second, the computer interface is presented to show how manual
123   annotation is integrated with the algorithm to train the detection procedure. Third, the procedure is validated
124   using data from the Ain River. The validation period occurred over six days in January and December 2012
125   where flow conditions ranged from ~$400 \ m^3/s$, which is below bankfull discharge but above the wood
126   transport threshold, to more than $800 \ m^3/s$. The developed algorithm can be used to characterize wood
127   pieces for a large image database at the study site. Future applications of this approach at a wide range of
128   sites should lead to new insights on the variability of wood pieces at the reach and watershed scales in world
129   rivers.

130   **2.   Methodological procedure for automatic detection of wood**

131   The algorithm for wood detection comprises a number of steps that seek to locate objects moving
132   through the field of view in a series of images and then identify the objects most likely to be wood. The
133   algorithm used in this work modifies the approach described by Ali *et al.*, (2011). The steps work from a
134   pixel to image to video scale, with the context from the larger scale helping to assess whether the information
135   at the smaller scale indicates the presence of floating wood or not. In a still image, a single pixel is charac-
136   terized by its location within the image, its color and its intensity. Looking at its surrounding pixels, on an
137   image scale, allows that information to be spatially contextualized. Meanwhile, the video data adds temporal
138   context, so that previous and future states of a given pixel can be used to assess its likeliness of representing
139   floating wood. Since an image is only a discrete 2D representation of the real 3D world, details about the
140   camera parameters such as optical image deformations, geographic situation, perspective deformations or
141   behavior regarding luminosity can be used to infer what wood should look like and where it should occur.
142   On a video scale, the method can embed expectations about how wood pieces should move through frames,
143   how big they should be, and how lighting and weather conditions can evolve to change the expectations of
144   wood appearance, location, and movement. The specific steps followed by the algorithm are shown in a
145   simple flow chart (Fig 1.a). An example image with a wood piece in the middle of the frame is also shown
146   for reference (Fig 1.b).

Fig 1

5

2.1. Wood probability masks

147

148   In the first step, each pixel was analyzed individually and independently. The static probability mask

149 answers the question "is one pixel likely to belong to a wood-block, given its color and intensity?". The

150 algorithm assumes that the wood pixels can be identified by pixel light intensity (x) following a Gaussian

151 distribution (Fig 2.a). To set the algorithm parameters, manual annotations of wood are used to obtain a

152 representative sample of wood pixels, from which both the mean (μ) and standard deviation (σ) are calcu-

153 lated. This procedure produces a static probability mask (Fig 2.b). From this figure, it is possible to identify

154 the sectors where wood presence is likely, which includes the floating wood piece seen in Fig 1.b, but also

155 includes standing vegetation in the lower part of the image and a shadowed area in the upper left. The ad-

156 vantage of this approach is that it is computationally very fast. However, misclassification is possible, par-

157 ticularly when light condition changes.

Fig 2

158   The second mask, called the dynamic probability mask, outlines each pixel's recent history. The corre-

159 sponding question is: "is this pixel likely to represent wood now, given its past and present characteristics?".

160 Again, this step is based on what is most common in our database: it is assumed that a wood pixel is darker

161 than a water pixel. Depending on lighting conditions like shadows cast on water or waves, this is not always

162 true, i.e. water pixels can be as dark as wood pixels. However, pixels displaying successively water then

163 wood tend to become immediately and significantly darker, while pixels displaying wood then water tend to

164 become significantly lighter. Meanwhile, pixels that keep on displaying wood tend to be rather stable. Thus,

165 we assign wood pixel probability according to an updated version of the function proposed by Ali et al.

166 (2011) (Fig 3.a) that takes 4 parameters. This function H is an updating function, which produces a temporal

167 probability mask from the inter-frame pixel value. On a probability map, a pixel value ranges from -1 (likely

168 not wood) to 1 (likely wood). The temporal mask value for a pixel at location (x, y) and at time t is

169 $P_T(x, y, t) = H(\Delta_t, I) + P_T(x, y, t - 1)$. We apply a threshold to the output of $P_T(x, y, t)$ so that it always

170 stays within the interval [0,1]. The idea is that a pixel that becomes suddenly and significantly darker is

171 assumed to be likely wood. $H(\Delta_t, I)$ is such that under those conditions, it increases the pixel probability map

172 value (parameters τ and β). A pixel that becomes lighter over time is unlikely to correspond to wood (pa-

173 rameter α). A pixel which intensity is stable and that was previously assumed to be wood shall still corre-

174 spond to wood, while a pixel which intensity is stable and which probability to be wood was low is unlikely

175 to represent wood now. A small decay factor (δ) was introduced in order to prevent divergence (in particular,

176   it prevents noisy areas from being activated too frequently).

Fig 3

177   The final wood probability mask is created using a combination of both the static and dynamic proba-

178   bility masks. Wood objects thus had to have a combination of the correct pixel color and the expected tem-

179   poral behavior of water-wood-water color. The masks were combined assuming that both probabilities are

180   independent, which allowed us to use the Bayesian probability rule in which the probability masks are simply

181   multiplied, pixel by pixel, to obtain the final probability value for each pixel of every frame.

2.2. Wood object identification and characterization

183   From the probability mask it is necessary to group pixels with high wood probabilities into objects and

184   then to separate these objects from the background to track them through the image frame. For this purpose,

185   pixels were classified as high-or low-probability based on a threshold applied to the combined probability

186   mask. Then, the high-probability pixels were grouped into connected components (that is, small, contiguous

187   regions on the image) to define the objects. At this stage, a pixel size threshold was applied on the detected

188   objects so that only the bigger objects were considered to represent woody objects on the water surface (Fig

189   4.a the big white region at the middle). A number of smaller components were often related to non-wood

190   objects, for example waves, reflections, or noise from the camera sensor or data compression.

191   After the size thresholding step, movement direction and velocity were used as filters to distinguish real

192   objects from false detections. The question here is, "is this object moving through the image frame the way

193   we would expect floating wood to move?". To do this, the spatial and temporal behavior of components were

194   analyzed. First, to deal with partly immersed objects, we agglomerated multiple objects within frames as

195   components of a single object if the distance separating them was less than a set threshold. Second, we asso-

196   ciated wood objects in successive frames together to determine if the motion of a given object was compatible

197   with what is expected from driftwood. This can be achieved according to the dimensionless parameter

198   "$PT/\Delta T$", which provides a general guideline for the distance an object pass between two consecutive frames

199   (Zhang et al., 2020). Here PT (passing time) is the time that one piece of wood passes through the camera

200   field of view and ΔT is the time between two consecutive frames and practically it is recommended to use

201   videos with $PT/\Delta T > 5$ in this software. In our case, tracking wood is rather difficult for classical object

202   tracking approaches in computer vision: the background is very noisy, the acquisition frequency is low and

203   the objects appearance can be highly variable due to temporarily submerged parts and highly variable 3D

204 structures. Given these considerations it was necessary to use very basic rules for this step. The rules are

205 therefore based on loose expectations, in terms of pixel intervals, on the motions of the objects, depending

206 on the camera location and the river properties. How many pixels is the object likely to move between image

207 frames from left to right? How many pixels from top to bottom? How many appearances are required? How

208 many frames can we miss because of temporary immersions? Using these rules, computational costs re-

209 mained low and the analysis could by run in real-time while also providing good performance.

Fig 4

210 The final step was to characterize each object, which at this point in the process are considered wood

211 objects. Each appears several times in different frames and a procedure is needed to either pick a single

212 representative occurrence or use a statistic tool to analyse multiple occurrences to estimate characterization

213 data. Here we assumed that the biggest occurrence, in terms of pixels number, was the most representative

214 state. This assumption is based on the principle that a bigger number of pixels corresponds to a better or a

215 fuller view (the object is less immersed than on other occurrences, for instance). This approach also matched

216 the manual annotation procedure where we tended to pick the view where the object covers the largest area

217 to make measurements. For the current paper, every object as characterized from the raw image based on its

218 size and its location (in pixels).

219 **2.3. Image rectification**

220 Warping images according to a perspective transform results in an important loss of quality. On warped

221 images, areas of the image farther to the camera provide little detail and are overall very blurry and non-

222 informative. Therefore, given the topology of our images, image rectification was necessary to calculated

223 wood length, velocity, volume and other characteristics from the saved pixel-based characterization of each

224 object. To do so, the fisheye lens distortion was first corrected. A fisheye lens distortion is a characteristic of

225 the lens that produces visual distortion intended to create a wide panoramic or hemispherical image. This

226 effect was corrected by a standard Matlab process using the ComputerVisionToolbox^{TM}.

227 Ground-based cameras have also an oblique angle of view, which means that pixel to meter correspond-

228 ence is variable and images need to be orthorectified to obtain estimates of object size and velocity in real

229 terms (Muste et al., 2008). Orthorectification refers to the process by which image distortion is removed and

230 the image scale is adjusted to match the actual scale of the water surface. Translating from pixels to cartesian

231 coordinates required us to assume that our camera follows the pinhole camera model and that the river can

232 be assimilated to a plane of constant altitude. Under such conditions, it is possible to translate from pixel

233 coordinates to a metric 2D space thanks to a perspective transform assuming a virtual pinhole camera on the

234 image and estimating the position of the camera and its principal point (center of the view). An example of

235 orthorectification on a detected wood piece in a set of continuous frames and pixel coordinates (Fig 5.b) is

236 presented in Fig 5.c in metrics coordinates. The transform matrix is obtained with the help of at least 4 non-

237 colinear points (Fig 5.a blue GCPs (Ground Control Points) acquired with DGPS) from which we know both

238 the relative 2D metric coordinates for a given water level (Fig 5.c blue points), and their corresponding lo-

239 calization within the image(Fig 5.b blue points). To achieve better accuracy, it is advised to acquire additional

240 points and to solve the subsequent over-determined system with the help of a Least Square Regression (LSR).

241 Robust estimators such as RANSAC can provide useful to prevent acquisition noise. After identifying the

242 virtual camera position, the perspective transform matrix then becomes parameterized with the water level.

243 Handling the variable water level was performed for each piece of wood, by measuring the relative height

244 between the camera and the water level at the time of detection based on information recorded at the gauging

245 station to which the camera was attached.

Fig 5

246 **3.   User interface**

247 The software was developed to provide a single environment for the analysis of wood pieces on the

248 surface of the water from streamside videos. It consists of four distinct modules: Detection, Annotation,

249 Learning, and Performance. The home screen (Fig 6) allows the operator to select any of these modules.

250 From within a module, a menu bar on the left side of the interface allows operators to switch from one module

251 to another. In the following sections, the operation of each of these modules are described.

Fig 6

252 **3.1. Detection**

253 The detection module is the heart of the software. This module allows, from learned or manually spec-

254 ified parameters, the detecting of floating objects without human intervention (see Fig 7). This module con-

255 tains two main parts: (i) Detection tab, which allows operator to open, analyze and export the results from

256 one video or a set of videos, and (ii) Configuration tab, which allows operator to load and save the software

257 configuration by defining the parameters of wood detection (as described in Sect 2), saving and extracting

258 the results, and displaying the interface.

259   The detection process is intended to work as a video file player. The idea is to load a video file (or a

260   stream url), and to let the software read the video until the end. When required, the reader generates a visual

261   output, showing how the masks behave by adding color and information to the video content (see Figure 7).

262   A small textual display area shows the frequency of past detections. Meanwhile, the software generates a

263   series of files summarizing the positive outputs of the detection. They consist in YAML and CSV files, as

264   well as image files to show the output of different masks, the original frames, etc. A configuration tab is

265   available, and provides many parameters organized by various categories. The main configuration tab is

266   divided in seven parts. The first part is dedicated to general configurations such as frame skipped between

267   each computation and defining the areas within the frame where wood is not expected (e.g. bridge pier or

268   river bank). In the second and third parts, the parameters of the intensity and temporal masks are listed (see

269   Sect 2.1). The default values are $\mu = 0.2$ and $\sigma = 0.08$ for the intensity mask, and $\tau = 0.25$ and $\beta = 0.45$

270   for the temporal mask. In the fourth and fifth parts, object tracking and characterization parameters are de-

271   fined respectively as described in Sect 2.2. Detection time is defined in the sixth part using an optical char-

272   acter recognition technique. Finally, the parameters of the orthorectification (see Sect 2.3) are defined in the

273   seventh part. The detection software can be used to process videos in batch ("script" tab), without generating

274   a visual output to save computing resources.

Fig 7

275   **3.2.   Annotation**

276   As mentioned in Sec. 2, the detection procedure requires the classification of pixels and objects into

277   wood and non-wood categories. To train and validate the automatic detection process, a ground-truth or set

278   of videos with manually annotations are required. Such annotations can be performed using different tech-

279   niques. For example, objects can be identified with the help of a bounding box or selection of endpoints, as

280   in MacVicar and Piégay(2012); Ghaffarian et al., (2020) and Zhang et al., (2020). It is also possible to sample

281   wood pixels without specifying instances or objects, or to sample pixels within annotated objects. Finally,

282   objects and/or pixels can be annotated multiple times in a video sequence to increase the amount and detail

283   of information in such an annotation database. However, this annotation process is time-consuming, so a

284   trade-off must be made between training and accuracy for different lighting conditions, camera parameters,

285   wood properties, and river hydraulics.

286   Given that the tool is meant to be as flexible as possible, the annotation tool was developed to allow

287   operator to perform as fine annotation as they wish. As it is shown in Fig 8, this module contains three main

288   parts: (i) The column on the far left allows operator to switch to another module (detection, learning or per-

289   formance), (ii) the central part consists of a video player with a configuration tab for extracting the data, and

290   (iii) the right part where the tools to generate, create, visualize and save annotations are located. The tools

291   allow rather quick coarse annotation, similar to what was done by MacVicar and Piégay (2012) and Boivin

292   *et al.,* (2015), while still allowing the possibility of finer pixel-scale annotation.

Fig 8

293   The principle of this module is to associate annotations with the frames of a given video. Annotating a

294   piece of wood is like drawing its shape, directly on a frame of the video, using the drawing tools provided by

295   the module. It is possible to add a text description to each annotation. Each annotation is linked to a single

296   frame of the video; however, a frame can contain several annotations. An annotated video, therefore, consists

297   of a video file, as well as a collection of drawings, possibly with textual descriptions, associated with frames.

298   It is possible to link annotations from one frame to another to signify that they belong to the same piece of

299   wood. These data can be used to learn the movement of pieces of wood in the frame.

3.3.   Performance

301   The performance module allows the operator to set rules to compare automatic and manual wood de-

302   tection results. This section also allows the operator to use a bare, pixel-based annotation or specify an or-

303   thorectification matrix to extract wood-size metrics directly from the output of an automatic detection.

304   For this module an automatic detection file is first loaded and then the result of this detection is com-

305   pared with a manual annotation for that video, if the latter is available. Comparison results are then saved in

306   the form of a summary file (*.csv format), allowing the operator to perform statistical analysis of the results

307   or the performance of the detection algorithm. A manual annotation file can only be loaded if it is associated

308   with an automatic detection result.

309   The performance of the detected algorithm can be realized on several levels:

310   • Object. The idea is to annotate one (or more) occurrences of a single object, and to operate the

311   comparison at bounding box scale. A detected object may comprehend a whole sequence of occur-

312   rences, on several frames. It is validated when only a single occurrence happens to be related to an

313   annotation. This is the minimum possible effort required to have an extensive overview of the

314   object frequency on such an annotations database. This approach can however lead us to misjudge

11

315   overall wrongly detected sequences as True Positives (see below), or vice-versa.

316   • Occurrence. The idea is to annotate, even roughly, every occurrence of every woody object, so that

317   the comparison can happen between bounding boxes rather than at pixel level. Every occurrence

318   of any detected object can be validated individually. This option requires substantially more anno-

319   tation work than the object annotation.

320   • Pixel. This case implies that every pixel of every occurrence of every object is annotated as wood.

321   It is very powerful in the event of evaluating the algorithm performances, and eventually refining

322   its parameters with the help of some machine learning technique. However, it requires an extensive

323   annotation work.

324   **4.   Performance assessment**

325   To assess the performance of the automatic detection algorithm, we used a set of videos from the Ain

326   River in France that were both comprehensively manually annotated and automatically analyzed. According

327   to the data annotated by the observer, the performance of the software can be affected by different conditions:

328   (i) wood piece length, (ii) distance from the camera, (iii, iv) wood X, Y position, (v) flow discharge, (vi)

329   daylight, and (vii, viii) light and darkness of the frame (see Table 2). If for example software detects a 1 cm

330   piece at a distance of 100 m from the camera, there is a high probability that this is a false positive detection.

331   Therefore, knowing the performance of the software in different conditions, it is possible to develop some

332   rules to enhance the quality of data. The advantage of this approach is that all eight parameters introduced

333   here are accessible easily in the detection process. In this section the monitoring details and annotation meth-

334   ods are introduced before the performance of the software is evaluated by comparing the manual annotations

335   with the automatic detections.

Table 2

336   **4.1. Material and methods**

337   **4.1.1. Monitoring site and annotation**

338   The Ain River is a piedmont river with a drainage area of 3630 km^2 at the gauging station of Chazey-

339   sur-Ain, with a mean flow width of 65 m, a mean slope of 0.15%, and a mean annual discharge of 120 m^3/s.

340   The lower Ain River is characterized by an active channel shifting within a forested floodplain (Lassettre et

341   al., 2008). An AXIS221 Day/Night^{TM} camera with a resolution of 768×576 pixels was installed at this station

342   to continuously record the water surface of the river at a maximum frequency of 5 fps (Fig 9). This camera

343   replaced a lower resolution camera at the same location used by MacVicar and Piégay (2012). The specific

344   location of the camera is on the outer bank of a meander, on the side closest to the thalweg, at a height of 9.8

345   m above the base flow elevation. The meander and a bridge pier upstream help to steer most of the floating

346   wood so that it passes relatively close to the camera where it can be readily detected with a manual procedure

347   (MacVicar and Piégay, 2012). The transformation matrix at the base flow elevation with the camera as the

348   origin is shown in Fig 10. Straight lines near the edges of the image appear curved because the fisheye

349   distortion has been corrected on this image (see Sect 2.3); conversely, a straight line, in reality, is presented

350   without any curvature in the image.

Fig 9

Fig 10

351   The survey period examined on this river was during 2012 from which two flood events, (January 1-7

352   and December 15) were selected for annotation. A range of discharges from $400 m^3/s$ to $800\ m^3/s$ occurred

353   during these periods (Fig 11), which is above a previously observed wood transport threshold of $\sim300\ m^3/s$

354   (MacVicar and Piégay, 2012). The flow discharge is available from the website (*www.hydro.eaufrance.fr*).

355   On January 3rd and 5th, a spider was active in front of the camera, which prevented a good video recording

356   and these days were therefore removed from the database. Detection was only possible during the daylight.

357   A summary of automated and manual detections for the six days is shown in Table 3.

Fig 11

358   **4.1.2. Assessment Methodology**

359   Ghaffarian et al. (2020), Zhang et al. (2020) show that the wood discharge can be measured from flux

360   or frequency of wood objects. An object level detection was thus sufficient for the larger goals of this re-

361   search at the Ain River, which is to get a complete budget of transported wood volume.

362   A comparison of annotated with automatic object detections gives rise to three options:

363   1- True Positive (TP): an object is correctly detected and is recorded in both the automatic and annotated

364   database

365   2- False Positive (FP): an object is incorrectly detected and is recorded only in the automatic database.

366   3- False Negative (FN): an object is not detected automatically and is only recorded in the annotated

13

367   database.

368   Despite overlapping occurrences of wood objects in the two databases, the objects could vary in position
369   and size between them. For the current study we set the TP threshold as the case where either at least 50%
370   of the automatic and annotated bounding box areas were common or at least 90% of an automatic bounding
371   box area was part of its annotated counterpart.

372   In addition to the raw counts of TPs, FPs, and FNs, we defined two measures of the performances of
373   the application, where:

374   • Recall Rate (RR) is the fraction of wood objects that are automatically detected ($TP/(TP + FN)$); and

375   • Precision Rate (PR) is the fraction of detected objects that are wood ($TP/(TP + FP)$).

376   The higher the PR and the RR are, the more accurate our application is. However, both rates tend to
377   interact. For example, it is possible to design an application that displays a very high RR (which means that
378   it doesn't miss many objects), but suffers from a very low PR (it outputs a high amount of inaccurate data),
379   and vice-versa. Thus, we have to find a balance that is appropriate to each application.

4.1.3. Factors used to understand variation in performance

381   It was well known from previous manual efforts to characterize wood pieces and develop automated
382   detection tools that it is easier to detect certain wood objects than others. In general, the ability to detect the
383   wood objects in the dynamic background of a river in flood was found to vary with the size of the wood
384   object, its position in the image frame, the flow discharge, the amount and variability of the light, interference
385   from other moving objects such as spiders, and other weather conditions such as wind and rain. In this section,
386   we describe and define the metrics that were used to understand the variability of the detection algorithm
387   performance.

388   In general, more light results in better detection. The light condition can be varied by variation of a set
389   of factors such as weather conditions or amount of sediment which is carried by the river. In any case, the
390   daylight is a factor that can change the light condition systematically, *i.e.* low light early in the morning (Fig
391   12.a), bright light at midday with potential for direct light and shadows (Fig 12.b), and low light again in the
392   evening, though different from the morning because the hue is more bluish (Fig 12.c). This effect of the time
393   of day was quantified simply by noting the time of the image, which was marked on the top of each frame of

14

394   the recorded videos.

Fig 12

395   Detection is also strongly affected by the frame 'roughness', defined here as the variation in light over

396   small distances in the frame. The change in light is important for the recognition of wood objects, but light

397   roughness can also occur when there is a region with relatively light pixels due to something such as reflection

398   of the surface of the water, and dark roughness can occur when there is a region with relatively dark pixels

399   due to something such as shadows from the surface water waves. Detecting wood is typically more difficult

400   around light roughness, which results in false negatives, while the color-map of a darker surface is often close

401   to that of wood, which results in false positives. Both of these conditions can be seen in Fig 12 which is

402   highlighted in Fig 12.a. In general, the frame roughness increases in windy days or when there is an obstacle

403   in the flow, such as downstream of the bridge pier in the current case. The light roughness was calculated for

404   the current study by defining a light intensity threshold and calculating the ratio of pixels of higher value

405   among the frame. The dark roughness is calculated in the same way, but in this case the pixels less than the

406   threshold were counted. In this work thresholds equal to 0.9 and 0.4 were used for light and dark roughness,

407   respectively.

408   The oblique view of the camera means that the distance of the wood piece from the camera is another

409   important factor in detection (Fig 13). The effect of distance on detection interacts with wood length, *i.e.*

410   shorter pieces of wood that are not detectable near the camera may not be detectable toward the far bank due

411   to the pixel size variation (Ghaffarian et al., 2020). Moreover, if a piece of wood passes through a region

412   with high roughness (Fig 13) or amongst bushes or trees (Fig 13 right hand side) it is more likely that the

413   software is unable to detect it. In our case, one day of video record could not be analyzed due to the presence

414   of a spider that moved around in front of the camera.

Fig 13

415   Flow discharge is another key variable in wood detection. Increasing flow discharge generally means

416   that water levels are higher, which brings wood close to the near bank of the river closer to the camera. This

417   change can make small pieces of wood more visible, but it also reduces the angle between the camera position

418   and pixels, which makes wood farther from the camera harder to see. High flows also tend to increase surface

419   waves and velocity, which can increase the roughness of the frame and lead to the wood being intermittently

420   submerged or obscured. More suspended sediment is carried during high flows which can change water

15

421   surface color and increase the opacity of the water.

4.2. Detection performance

423   Automatic detection software performance was evaluated based on the event based TP, FP, and FN

424   raw numbers and the precision (PR) and recall rates (RR) using the default parameters in the software. On

425   average, manual annotation resulted in the detection of approximately twice as many wood pieces as the

426   detection software (Table 3). Measured over all the events, RR = 29%, which indicates that many wood

427   objects were not detected by the software, while among detected objects about 36% were false detections

428   ($PR = 64\%$).

Table 3

429   To better understand model performance, we first tested the correlation between the factors identified

430   in the previous section (Table 4). As shown, the pairs of dark/light roughness, length/distance and dis-

431   charge/time were highly correlated ($Corr. = 0.59, 0.46, 0.37$ respectively). For this reason, they were con-

432   sidered together to evaluate the performance of the algorithm within a given parameter space. The X/Y po-

433   sitions were also considered as a pair despite a relatively low correlation (0.15) because they represent the

434   position of an object. As a note, the correlation between time and dark roughness is higher than discharge

435   and time, but we used the discharge/time pair because discharge has a good correlation only with time. As

436   recommended by MacVicar and Piégay (2012), wood lengths were determined on a log base 2 transformation

437   to better compare different classes of floating wood, similar to what is done for sediment sizes.

Table 4
Fig 14

438   The presentation of model performance by pairs of correlated parameters clarifies certain strengths and

439   weaknesses of the software (Figure 14). As expected, the results of Fig 14.b indicate that first, the software

440   is not so precise for small pieces of wood (less than the order of 1 m), and second there is an obvious link

441   between wood length and the distance from the camera so that by increasing the distance from the camera,

442   the software is precise only for larger pieces of wood. Based on Fig 14.e, the software precision is usually

443   better on the right side of the frame than the left side. It would be reasonable, as the software requires to

444   detect a patch at least in 5 continuous frames to recognize it as a piece of wood (see Sect 2.2 and Fig 4 for

445   more information). Therefore, most of the true positives are on the right side of the frame, where 5 continuous

446   frames have already established. Also, the presence of the bridge pier (at X ≅ -30 to -40 m based on Fig 10)

16

447 in the upstream, produces lots of waves that decreases the precision of the software. Also, Fig 14.h shows

448 that the software is much more precise during the morning when there is enough light rather than evening

449 when the sunshine decreases. However, at low flow ($Q < 550\ m^3/s$) the software precision decreases sig-

450 nificantly. Finally, based on Fig 14.k, the software does not work well in two roughness conditions: (i) in a

451 dark smooth flow (light roughness $\cong 0$) when there are some dark patches (shadows) on the surface (dark

452 roughness $\cong 0.3$), and (ii) when both roughness increases and there are many noises in a frame.

453   To estimate the fraction of wood pieces that the software did not detect, the recall rate RR is calculated

454 in different conditions and a linear interpolation was applied on RR as it is presented in Fig 14, third column.

455 According to Fig 14.c, RR is fully dependent on piece length so that for the lengths at the order of 10 m ($L =$

456 $O(10)$) RR is very good. By contrast when $L = O(0.1{\sim}1)$ the RR is too small. There is a transient region

457 when $L = O(1)$ which is slightly depends on the distance from the camera. One can say, the wood length is

458 the most crucial parameter that affects the recall rate independent of the operator annotation. Based on Fig

459 14.f, the RR is much better on the left side of the frame than on the right side. It can be because the operator's

460 eye needs some time to detect a piece of wood, so most of the annotations are on the right side of the frame.

461 Having a small number of detections on the left side of the frame results in the small value of FN which

462 followed by high values of RR in this region ($RR = TP/(TP + FN)$). Therefore, while the position of detec-

463 tion plays a significant role in the recall rate, it is completely dependent on the operator bias. By contrast,

464 frame roughness, daytime, and flow discharge do not play a significant role in the recall rate (Fig 14. i, l).

465 **4.3. Post-processing**

466   This section is separated into two main parts. First, we show how to improve the precision of the soft-

467 ware by a posteriori distinction between TP and FP. After removing FPs from the detected pieces, in the

468 second part, we test a process to predict the annotated data that the software missed *i.e.* false negatives.

469 **4.3.1. Precision improvement**

470   To improve the precision of the automatic wood detection we first ran the software to detect pieces and

471 extracted the eight key parameters for each piece as described in Sect 4.1.3. We then estimated the total

472 precision of each object, as the average of four precisions from each sub-figure of Fig 14. In the current study

473 the detected piece was considered to be a true positive if the total precision exceeded 50%. To check the

474 validity of this process, we used cross-validation by leaving one day out, calculating the precision matrices

475 based on five other days, and applying the calculated PR matrices on the day that was left out. As is seen in

17

476   Table 5, this post-processing step increases the precision of the software to 85%, an enhancement of 21%.

477   The degree to which the precision is improved is dependent on the day left out for cross-validation. If, for

478   example, the day left out had similar conditions to the mean, the PR matrices were well trained and were able

479   to distinguish between TP and FP (*e.g.* 2nd Jan with 42% enhancement). On the other hand, if we have an

480   event with new characteristics (*e.g.* very dark and cloudy weather or at discharges different from what we

481   have in our database), the PR matrices were relatively blind and offered little improvement (*e.g.* 15th Dec

482   with 10% enhancement).

Table 5

483   One difficulty with the post-processing reclassification of wood piece is that this new step can also

484   introduce error by classifying real objects as false positives (making them a false negative) or vice-versa.

485   Using the training data, we were able to quantify this error and categorized them as post-processed false

486   negatives ($\textbf{\textit{FN}}_{\textbf{\textit{pp}}}$) with an associated recall rate ($\textbf{\textit{RR}}_{\textbf{\textit{pp}}}$). As shown in Table 5, the precision enhancement

487   process lost only around 14% of TPs (RR_{pp}= 86%).

488   Instead of using all eight key parameters (four PR matrices) to calculate the overall precision, it is also

489   possible to use other configurations by combining different matrices as it is shown in Fig 15. In this figure,

490   the precision matrices 1 to 4 are the same as the matrices presented in Fig 14 and different colors show

491   different combinations of these matrices. As it is seen, some configurations (e.g. (2,4) or (1,3,4)) result in

492   better precision and some cases (e.g. (1,2) or (1,3)) there is almost no difference between post-processed PR

493   and the raw data. The reason that configurations like (2,4) or (1,3,4) with a better precision rate were not used

494   here was that in these cases the post-processed recall rate RR_{pp} was low (around 60%) meaning that by using

495   these configurations many of true positives was removed. Therefore, to have the best precision enhancement

496   with maximum post-processed recall rate all 4 different precision matrices are used (Fig 15, dark red scatters).

Fig 15

497   **4.3.2.   Modeling missed wood pieces based on the recall rate**

498   The automated software detected 29% of the number of manually annotated wood pieces (Table 5). In

499   the previous section, it was described how to enhance the precision of the software to ensure that these auto-

500   matically detected pieces are TPs. The larger question, however, is how to model the missing pieces. Based

501   on Fig 14, the software work well for very large objects in most areas of the image and in most lighting

502   conditions. However, the smaller pieces were found to be harder to detect, making the wood length the most

503   important factor governing the recall rate. Based on this idea, the final step in the post processing is to apply

504   a model to account for the smaller wood pieces.

505   The model is based on the concept of a threshold piece length. Above the threshold, wood pieces are

506   likely to be accurately counting using the automatic software. Below the threshold, on the other hand, the

507   automatic detection software is likely to deviate from the manual counts. The actual length distribution was

508   first determined based on the manual annotations ($TP + FN$) (Fig 16.a). Also shown are the raw results of

509   the automatic detection software ($TP + FP$) and the raw results with the false positives removed (TP). At

510   this stage, the difference between the TP and the $TP + FN$ lines are the false negatives (FN) that the software

511   has missed. Comparison between the two lines shows that they tend to deviate between 2-3 m. The correla-

512   tion coefficient between them was calculated for thresholds varying from 1 cm to 15 m length and 2.5 m

513   length was defined as the optimum threshold length for recall modeling (Fig 16.b).

514   In the next step we wanted to estimate the pieces less than 2.5 m that the software missed. During the

515   automatic detection process, when the software detects a piece of wood, according to Fig 14 (third column),

516   the RR can be calculated for this piece (same protocol as precision enhancement in Sect 4.3.1). Therefore, if

517   for example the average recall rate for a piece of wood is 50%, there is likely to be another piece in the same

518   condition (defined by the eight different parameters described in Table 2) that the software could not detect.

519   To correct for these missed pieces, additional virtual pieces were added to the database. Fig 16.a, shows the

520   length distribution after adding these virtual pieces to the database (blue line, total of 5841 pieces). The result

521   shows a good agreement between this and the operator annotations (green line, total of 6249 pieces), which

522   results in a relative error of only 6.5% in the total number of wood pieces.

Fig 16

523   On the Ain River by separating videos to 15 min segments, MacVicar and Piégay, (2012) and Zhang et

524   al., (2020) proposed the following equation for calculating wood discharge from the wood flux:

525          $$Q_w = 0.0086F^{1.24} \qquad\qquad\qquad (1)$$

526   where, Q_w is the wood discharge ($m^3/15min$) and F is the wood flux (piece number/15 min). Using

527   this equation, the total volume of wood was calculated based on three different conditions: (i) operator anno-

528   tation ($TP + FN$), (ii) raw data of the detection software ($TP + FP$) and (iii) post-processed data of the de-

529   tection software ($TP_{modeled}$). Fig 17 shows a comparison of the total volume of wood from the manual

19

530   annotations in comparison with the raw and post-processed annotations from the detection software. As
531   shown, the raw detection results underestimate wood volume by almost one order of magnitude. After pro-
532   cessing, the results show some scatter but are distributed around the 1:1 slope, which indicates that they
533   follow the manual annotation results. There is a slight difference for days with lower fluxes (Jan 4 and 7),
534   where the post-processing tends to over-estimate wood volumes, but in terms of an overall wood balance the
535   volume of wood on these days are negligible. In total, 125 m^3 wood was annotated by the operator and the
536   software automatically detected only 46 m^3, some of which represent false positives. After post-processing,
537   142 m^3 wood was estimated to have passed in the analyzed videos for a total error of 13.5%.

Fig 17

538   **5.   Conclusion**

539   Here, we present new software for the automatic detection of wood pieces on the river surface. After
540   presenting the corresponding algorithm and the user interface, an example of automatic detection was pre-
541   sented. We annotated 6 days of flood events that were used to first check the performance of the software
542   and then develop post-processing steps to both remove possibly erroneous data and model data that were
543   possibly missed by the software.

544   To evaluate the performance of the software, we used precision and recall rates. The automatic detection
545   software detects around one third of all annotated wood pieces with 64% precision rate. Then using the op-
546   erator annotations as the ultimate goal, the post-processing part was applied to extrapolate data extracted
547   from detection results, aiming to come as close as possible to the annotations. It is shown that using four pair
548   of key factors: (i) light and dark roughness of the frame, (ii) daytime and flow discharge, (iii) X, Y coordinates
549   of detection position, and (iv) distance of detection as a function of piece length, it is possible to detect false
550   positives and increase the software precision to 86%. Using the concept of a threshold piece length for de-
551   tection it is shown that it is then possible to model the missed wood pieces (false negatives). In the presented
552   results, the final recall rate results in a relative error of only 6.5% for piece number and 13.5% for wood
553   volume.

554   This work shows the feasibility of the detection software to detect wood pieces automatically. Auto-
555   mation will significantly reduce the time and expertise required for manual annotation, making video moni-
556   toring a powerful tool for researchers and river managers to quantify the amount of wood in rivers. The

Earth **Surface**
Dynamics
Discussions

557 software should be applied in other rivers to test it in different contexts and enhance its accuracy.

6. Code/Data/Sample availability

559   Not available.

7. Author contribution

561 Hossein Ghaffarian: Application of statistical, and computational techniques to analyses study data. Creation
562 and presentation of the published work.

563 Hervé Piégay, Bruce MacVicar, Hossein Ghaffarian: Development and design of methodology; creation of
564 models.

565 Laure Tougne, Pierre Lemaire: Programming and software development.

566 Pierre Lemaire, Zhang Zhi: Performing the surveys, and data collection.

567 Hervé Piégay, Bruce MacVicar, Pierre Lemaire, Hossein Ghaffarian: Critical review, commentary, and revi-
568 sion.

569 Hervé Piégay: Oversight and leadership responsibility for the research activity planning and execution, in-
570 cluding mentorship external to the core team.

8. Competing interests

572   The authors declare that they have no conflict of interest.

9. Acknowledgment

21

Earth **Surface**
Dynamics
Discussions

Open Access

EGU

578 **10.   References**

579   Abbe TB, Montgomery DR. 2003. Patterns and processes of wood debris accumulation in the Queets
580 river basin, Washington. *Geomorphology* **51** : 81–107.

581   Ali I, Mille J, Tougne L. 2011. Wood detection and tracking in videos of rivers. In *Scandinavian Con-*
582 *ference on Image Analysis*, pp. 646–655. Springer, Springer Berlin Heidelberg.

583   Ali I, Mille J, Tougne L. 2012. Space–time spectral model for object detection in dynamic textured
584 background. *Pattern Recognition Letters* **33** : 1710–1716.

585   Ali I, Mille J, Tougne L. 2014. Adding a rigid motion model to foreground detection: application to
586 moving object detection in rivers. *Pattern Analysis and Applications* **17** : 567–585.

587   Ali I, Tougne L. 2009. Unsupervised Video Analysis for Counting of Wood in River during Floods. *In*
588 *Advances in Visual Computing,* Bebis G et al. (eds). Springer Berlin Heidelberg: Berlin, Heidelberg; 578–
589 587.

590   Badoux A, Andres N, Turowski JM. 2014. Damage costs due to bedload transport processes in Swit-
591 zerland. *Natural Hazards and Earth System Sciences (NHESS)* **14** (2), 279–294.

592   Benacchio V, Piégay H, Buffin-Bélanger T, Vaudor L. 2017. A new methodology for monitoring wood
593 fluxes in rivers using a ground camera: Potential and limits. *Geomorphology* **279** : 44–58.

594   Benacchio V, Piégay H, Buffin-Belanger T, Vaudor L, Michel K. 2015. Automatioc imagery analysis
595 to monitor wood flux in rivers (Rhône River, France). *Presented at the 2015 Third International Conference*
596 *Wood In World Rivers*, 6 July, Padova, Italy. Available from: http://www.sedalp.eu/events/dwd/proceed-
597 ings_WWR32015.pdf

598   Boivin M, Buffin-Bélanger T, Piégay H. 2015. The raft of the Saint-Jean River, Gaspé (Québec, Can-
599 ada): A dynamic feature trapping most of the wood transported from the catchment. *Geomorphology* **231** :
600 270–280.

601   Boivin M, Buffin-Bélanger T, Piégay H. 2017. Interannual kinetics (2010–2013) of large wood in a
602 river corridor exposed to a 50-year flood event and fluvial ice dynamics. *Geomorphology* **279** : 59–73.

603   Braudrick CA, Grant GE. 2000. When do logs move in rivers? *Water Resources Research* **36** : 571–
604   583.

605   Cerutti G, Tougne L, Mille J, Vacavant A, Coquin D. 2013. Understanding leaves in natural images–a
606   model-based approach for tree species identification. *Computer Vision and Image Understanding* **117** : 1482–
607   1501.

608   Cerutti G, Tougne L, Vacavant A, Coquin D. 2011. A parametric active polygon for leaf segmentation
609   and shape estimation. In *International symposium on visual computing*, pp. 202–213. Springer.

610   Comiti F, Andreoli A, Lenzi MA, Mao L. 2006. Spatial density and characteristics of woody debris in
611   five mountain rivers of the Dolomites (Italian Alps). *Geomorphology* **78** : 44–63.

612   De Cicco PN, Paris E, Ruiz-Villanueva V, Solari L, Stoffel M. 2018. In-channel wood-related hazards
613   at bridges: A review: In-channel wood-related hazards at bridges: A review. *River Research and Applications*
614   **34** : 617–628.

615   Ghaffarian H, Piégay H, Lopez D, Rivière N, MacVicar B, Antonio A, Mignot E. 2020. Video-moni-
616   toring of wood discharge: first inter-basin comparison and recommendations to install video cameras. Earth
617   Surface Processes and Landforms Available from: https://onlinelibrary.wiley.com/doi/abs/10.1002/esp.4875

618   Gordo A, Almazán J, Revaud J, Larlus D. 2016. Deep image retrieval: Learning global representations
619   for image search. In *European conference on computer vision*, pp. 241–257. Springer.

620   Gregory S, Boyer KL, Gurnell AM. 2003. Ecology and management of wood in world rivers. In *Amer-
621   ican Fisheries Society, Bethesda, USA*, , vol. 23, pp. 663–665.

622   Gurnell AM, Piégay H, Swanson FJ, Gregory SV. 2002. Large wood and fluvial processes. *Freshwater
623   Biology* **47** : 601–619.

624   Haga H, Kumagai T, Otsuki K, Ogawa S. 2002. Transport and retention of coarse woody debris in
625   mountain streams: An in situ field experiment of log transport and a field survey of coarse woody debris
626   distribution. *Water Resources Research* **38** : 1-1.

627   Jacobson PJ, Jacobson KM, Angermeier PL, Cherry DS. 1999. Transport, retention, and ecological

628   significance of woody debris within a large ephemeral river. *Journal of the North American Benthological*
629   *Society* **18** : 429–444.

630   Keller EA, Swanson FJ. 1979. Effects of large organic material on channel form and fluvial processes.
631   *Earth Surface Processes and Landforms* **4** : 361–380.

632   Kramer N, Wohl E. 2014. Estimating fluvial wood discharge using time-lapse photography with varying
633   sampling intervals. *Earth Surface Processes and Landforms* **39** : 844–852.

634   Kramer N, Wohl E, Hess-Homeier B, Leisz S. 2017. The pulse of driftwood export from a very large
635   forested river basin over multiple time scales, Slave River, Canada. *Water Resources Research* **53**(3) : 1928–
636   1947.

637   Lagasse PF. 2010. Effects of debris on bridge pier scour, , vol. 653. Transportation Research Board

638   Lassettre NS, Piégay H, Dufour S, Rollet A-J. 2008. Decadal changes in distribution and frequency of
639   wood in a free meandering river, the Ain River, France. *Earth Surface Processes and Landforms* **33** : 1098–
640   1112.

641   Lejot J, Delacourt C, Piégay H, Fournier T, Trémélo M-L, Allemand P. 2007. Very high spatial resolu-
642   tion imagery for channel bathymetry and topography from an unmanned mapping controlled platform. *Earth*
643   *Surface Processes and Landforms* **32** (11): 1705–1725.

644   Lemaire P, Piégay H, MacVicar B, Mouquet-Noppe C, Tougne L. 2014. Automatically monitoring
645   driftwood in large rivers: preliminary results. *Presented at the 2014 AGU Fall Meeting*. 19 December, San
646   Francisco, USA. Available from: https://agu.confex.com/agu/fm14/meetingapp.cgi/Paper/22487

647   Lienkaemper GW, Swanson FJ. 1987. Dynamics of large woody debris in streams in old-growth Doug-
648   las-fir forests. Canadian Journal of Forest Research **17** (2): 150–156.

649   Liu L, Ouyang W, Wang X, Fieguth P, Chen J, Liu X, Pietikäinen M. 2020. Deep learning for generic
650   object detection: A survey. *International journal of computer vision* **128** : 261–318.

651   Lucía A, Comiti F, Borga M, Cavalli M, Marchi L. 2015. Dynamics of large wood during a flash flood
652   in two mountain catchments. *Natural Hazards and Earth System Sciences* **15** (8): 1741.

24

Earth **Surface**
Dynamics
Discussions

653   Lyn D, Cooper T, Yi Y-K. 2003. Debris accumulation at bridge crossings: laboratory and field studies
654   . Purdue University: West Lafayette. Available from: http://docs.lib.purdue.edu/jtrp/48

655   MacVicar B, Piégay H. 2012. Implementation and validation of video monitoring for wood budgeting
656   in a wandering piedmont river, the Ain River (France). *Earth Surface Processes and Landforms* **37** (12):
657   1272–1289.

658   MacVicar BJ, Piégay H, Henderson A, Comiti F, Oberlin C, Pecorari E. 2009a. Quantifying the tem-
659   poral dynamics of wood in large rivers: field trials of wood surveying, dating, tracking, and monitoring tech-
660   niques. *Earth Surface Processes and Landforms* **34** (15): 2031–2046.

661   MacVicar BJ, Piégay H, Tougne L, Ali I. 2009b. Video monitoring of wood transport in a free-mean-
662   dering piedmont river. In *AGU Fall Meeting Abstracts*.

663   Mao L, Comiti F. 2010. The effects of large wood elements during an extreme flood in a small tropical
664   basin of Costa Rica. *WIT Transactions on Engineering Sciences* **67** : 225–236.

665   Marcus WA, Legleiter CJ, Aspinall RJ, Boardman JW, Crabtree RL. 2003. High spatial resolution hy-
666   perspectral mapping of in-stream habitats, depths, and woody debris in mountain streams. *Geomorphology*
667   **55** (1-4): 363–380.

668   Marcus WA, Marston RA, Colvard Jr CR, Gray RD. 2002. Mapping the spatial and temporal distribu-
669   tions of woody debris in streams of the Greater Yellowstone Ecosystem, USA. *Geomorphology* **44** (3-4):
670   323–335.

671   Martin DJ, Benda LE. 2001. Patterns of Instream Wood Recruitment and Transport at the Watershed
672   Scale. *Transactions of the American Fisheries Society* **130** (5): 940–958.

673   Mazzorana B, Ruiz-Villanueva V, Marchi L, Cavalli M, Gems B, Gschnitzer T, Mao L, Iroumé A,
674   Valdebenito G. 2018. Assessing and mitigating large wood-related hazards in mountain streams: recent ap-
675   proaches. *Journal of Flood Risk Management* **11** (2): 207–222.

676   Moulin B, Piégay H. 2004. Characteristics and temporal variability of large woody debris trapped in a
677   reservoir on the River Rhone(Rhone): implications for river basin management. *River Research and*

678   *Applications* **20** (1): 79–97.

679   Muste M, Fujita I, Hauet A. 2008. Large-scale particle image velocimetry for measurements in riverine
680   environments. *Water Resources Research* **44** (W00D19)

681   Piégay H, Lemaire P, MacVicar B, Mouquet-Noppe C, Tougne L. 2014. Automatically monitoring
682   driftwood in large rivers: preliminary results. In *AGU Fall Meeting Abstracts*.

683   Ravazzolo D, Mao L, Picco L, Lenzi MA. 2015. Tracking log displacement during floods in the Taglia-
684   mento River using RFID and GPS tracker devices. *Geomorphology* **228** : 226–233.

685   Roussillon T, Piégay H, Sivignon I, Tougne L, Lavigne F. 2009. Automatic computation of pebble
686   roundness using digital imagery and discrete geometry. *Computers & Geosciences* **35** (10): 1992–2000.

687   Ruiz-Villanueva V, Bodoque JM, Díez-Herrero A, Bladé E. 2014. Large wood transport as significant
688   influence on flood risk in a mountain village. *Natural hazards* **74** (2): 967–987.

689   Ruiz-Villanueva V, Bürkli L, Mazzorana B, Mao L, Ravazzolo D, Iribarren P, Wohl E, Nakamura F,
690   Stoffel M. 2018. Defining and characterizing wood-laden flows in rivers using home videos. In *E3S Web of*
691   *Conferences*, , vol. 40, p. 02014. EDP Sciences

692   Ruiz-Villanueva V, Piégay H, Gurnell AM, Marston RA, Stoffel M. 2016. Recent advances quantifying
693   the large wood dynamics in river basins: New methods and remaining challenges: Large Wood Dynamics.
694   *Reviews of Geophysics* **54** (3): 611–652.

695   Schenk ER, Moulin B, Hupp CR, Richter JM. 2014. Large wood budget and transport dynamics on a
696   large river using radio telemetry. *Earth Surface Processes and Landforms* **39** (4): 487–498.

697   Senter, A.E., Pasternack, G.B., Piégay, H., Vaughan, M.C. & Lehyan, J.S. 2017 Wood export varies
698   among decadal, annual, seasonal, and daily scale hydrologic regimes in a large, mediterranean climate, moun-
699   tain river watershed. *Geomorphology* **276**, 164–179.

700   Senter AE, Pasternack GB. 2011. Large wood aids spawning Chinook salmon (Oncorhynchus
701   tshawytscha) in marginal habitat on a regulated river in California. *River Research and Applications* **27** (5):
702   550–565.

26

703   Seo JI, Nakamura F. 2009. Scale-dependent controls upon the fluvial export of large wood from river

704   catchments. *Earth Surface Processes and Landforms* **34** (6): 786–800.

705   Seo JI, Nakamura F, Chun KW. 2010. Dynamics of large wood at the watershed scale: a perspective on

706   current research limits and future directions. *Landscape and Ecological Engineering* **6** (2): 271–287.

707   Seo JI, Nakamura F, Nakano D, Ichiyanagi H, Chun KW. 2008. Factors controlling the fluvial export

708   of large woody debris, and its contribution to organic carbon budgets at watershed scales. *Water Resources*

709   *Research* **44** (W04428)

710   Turowski JM, Badoux A, Bunte K, Rickli C, Federspiel N, Jochner M. 2013. The mass distribution of

711   coarse particulate organic matter exported from an Alpine headwater stream. Earth surface dynamics **1** (1):

712   1–11.

713   Viola PA, Jones MJ. 2006. Object recognition system. US Patent 7,031,499.

714   Warren DR, Kraft CE. 2008. Dynamics of large wood in an eastern US mountain stream. Forest Ecology

715   and Management **256** (4): 808–814.

716   Wohl E. 2013. Floodplains and wood. Earth-Science Reviews **123** : 194–212.

717   Wohl E, Scott DN. 2017. Wood and sediment storage and dynamics in river corridors. Earth Surface

718   Processes and Landforms **42** (1): 5–23.

719   Zhang Z, Ghaffarian H, MacVicar B, Vaudor L, Antonio A, Michel K, Piégay H. 2020. Video monitor-

720   ing of in-channel wood fluxes: critical events, flux prediciton and sampling window. *Earth Surface Processes*

721   *and Landforms*

722

Table 1 Characteristics of streamside video monitoring techniques in different studies.

Article	Sampling	Temporal scales	Camera resolution	Study site
MacVicar & Piégay (2012)	15 min segments	3 floods/18 hr/5 fps	640 × 480	Ain, France
Kramer & Wohl (2014)	Total duration	32 days/12761 frames/0.017 fps	n/a	Slave, Canada
Boivin et al. (2017)	Total duration	3 floods/150 hr/25 fps	640 × 480	St Jean, Canada
Kramer et al. (2017)	Total duration	11 months/0.0017 fps	1268 × 760	Slave, Canada
Senter et al. (2017)	15 min segments	39 days/180 hr/4 fps	2048 × 1536	North Yuba, USA
Ghaffarian et al. (2020)	Total duration	2 floods/80 hr/1 fps	600 × 800	Isère, France
Zhang et al. (2020)	Total duration	7 floods & 1 windy period /183 hr/5 fps	from 640 × 480 up to 800 × 600	Ain, France

Table 2 Parameters used to assess the performance of the software

Parameter	Rational	Metric
Piece length	Larger objects are easier to detect.	Detecting an object in pixel coordinates. Transferring coordinates to metric. Calculating length, position, and distance.
Distance	Objects closer to the camera are easier to detect.	
X position	Some particular areas of turbulent flow in the field of view affect detection (e.g. presence of a bridge pier).	
Y position		
Discharge	Flow discharge affects water color, turbulence and the amount of wood.	Recorded water elevation data and calibrated rating curve at hydrologic station.
Time	Luminosity of the frames varies with time of day.	Time of day as indicated on top of each frame.
Dark roughness	Small spots with sharp contrast (either lighter or darker) affect detection.	% of pixels below an intensity threshold
Light roughness		% of pixels above an intensity threshold

723

Table 3 Summary of automated and manual detections

Date	discharge (m^3/s)		Water level (m)		Detection time (hr)	Number		Precision rate%	Recall rate%
	Q_{max}	Q_{min}	h_{max}	h_{min}		annot.	det.		
1/1/2012	718	633	-7.4	-7.8	7 to 17	2282	972	77	33
2/1/2012	772	674	-7.2	-7.6	7 to 17	802	380	52	24
4/1/2012	475	423	-8.4	-8.6	7 to 17	140	158	20	22
6/1/2012	786	763	-7.2	-7.2	7 to 17	712	384	54	29
7/1/2012	462	430	-8.5	-8.6	7 to 17	117	73	40	25
15/12/2012	707	533	-7.5	-8.2	9 to 14	1296	503	72	28
Total	786	423	-7.2	-8.6	55 hr	5349	2470	64	29

724

28

Table 4 Correlation between parameters

	Dark roughness	Light roughness	Length	Distance	X position	Y position	Discharge	Time
Dark roughness		0.59	-0.02	-0.04	0.04	0.1	0	0.57
Light roughness	0.59		-0.03	-0.03	0.03	0.09	-0.04	0.29
Length	-0.02	-0.03		0.46	-0.45	-0.35	-0.02	-0.01
Distance	-0.04	-0.03	0.46		-1	-0.16	0.14	-0.05
X position	0.04	0.03	-0.45	-1		0.15	-0.15	0.05
Y position	0.1	0.09	-0.35	-0.16	0.15		0	0.07
Discharge	0	-0.04	-0.02	0.14	-0.15	0		0.37
Time	0.57	0.29	-0.01	-0.05	0.05	0.07	0.37	

Table 5 Precision rate (PR) before and after post-processing

		1 Jan	2 Jan	4 Jan	6 Jan	7 Jan	15 Dec	Total
Raw data	TP	745	196	31	206	29	363	1570
	FP	227	184	127	178	44	140	900
	FN	1537	606	109	506	88	933	3779
	$PR\%$	77	52	20	54	40	72	64
	$RR\%$	33	24	22	29	25	28	29
Post-proc.	TP	658	150	30	178	22	315	1353
	FP	64	10	60	39	11	68	252
	FN_{pp}[1]	87	46	1	28	7	48	217
	$PR\%$	91	94	33	82	67	82	85
	RR_{pp}[2]$\%$	88	77	97	86	76	87	86
PR improvement		14	42	13	28	27	10	21

725   [1] FN_{pp} denotes the false estimations of the precision matrices which results in missing some TP.

726   [2] RR_{pp} denotes the recall rate of post processing which corresponds to FN_{pp}.

727
728
729
730

731

a)

Original image

Static mask   Dynamic mask

Combined mask

↓

Object extraction

↓

Object tracking

↓

Characterization

↓

Orthorectification

b)
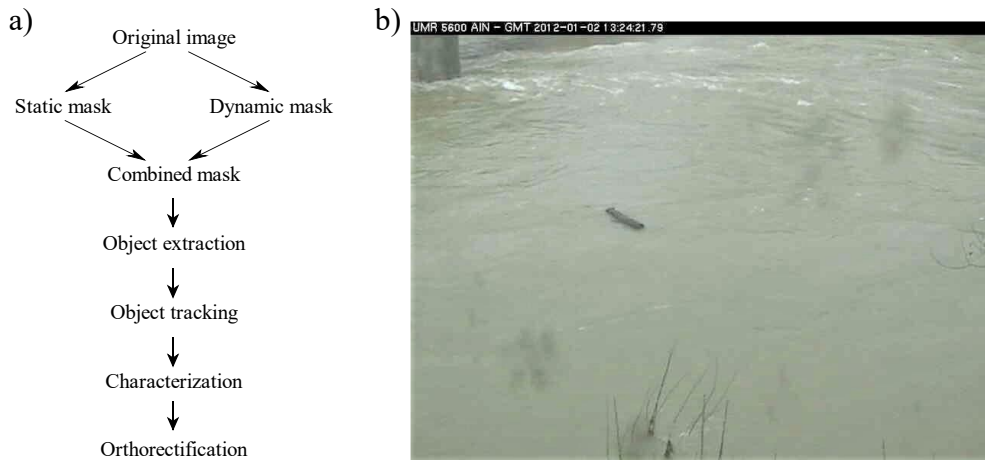
732

Fig 1 a) Flowchart of the detection software and b) an example of frame on which these different flowchart steps are applied.

a)

$$f(x|\mu,\sigma^2) = \frac{1}{\sqrt{2\sigma^2\pi}} e^{-\frac{(x-\mu)^2}{2\sigma^2}}$$

Light intensity for wood

PDF

light intensity

b)
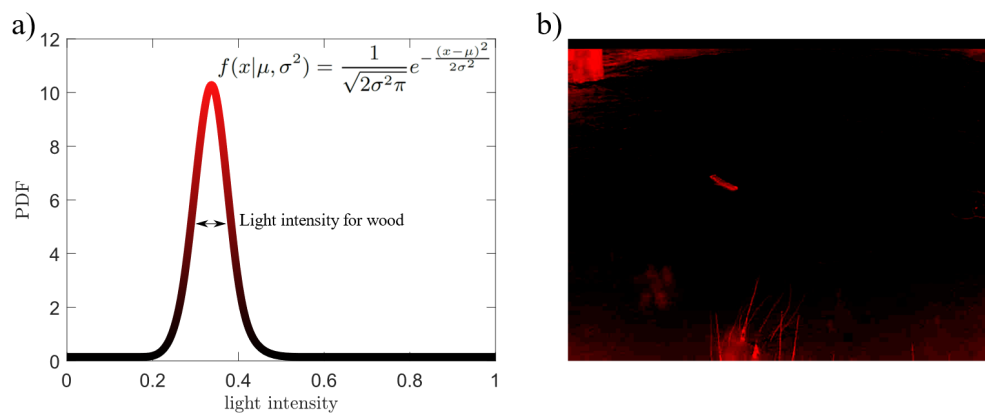
733

Fig 2 Static probability mask, a) Gaussian distribution of light intensity range for a piece of wood, b) employment of probability mask on the sample frame.

a)

734

b)
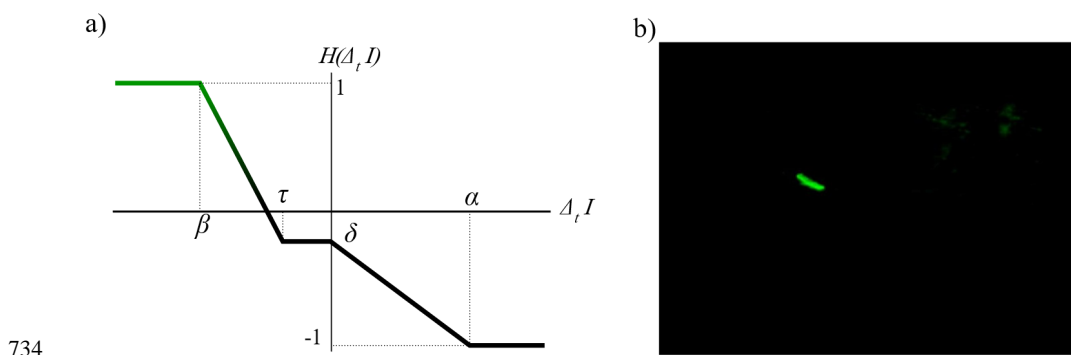
Fig 3 Dynamic probability mask, a) updating function $H(\Delta_t, I)$ adapted from Ali et al. (2011) and b) employment of probability mask on the sample frame.

a)

b)

735
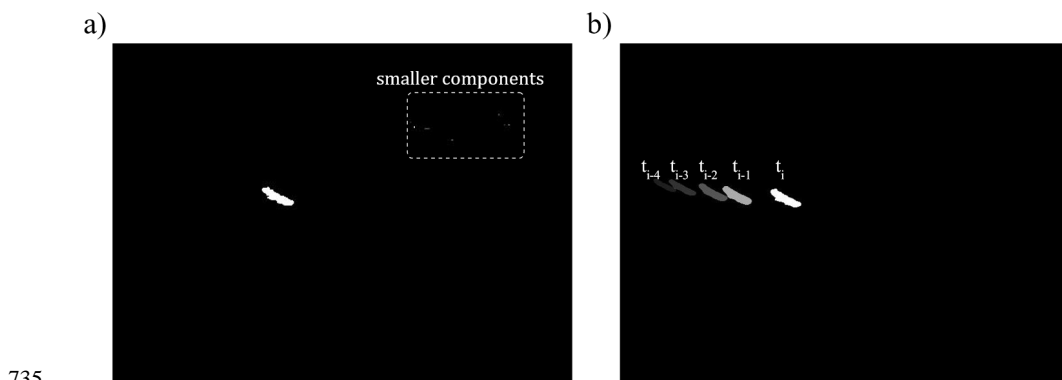
Fig 4 a) Object extraction by (i) combining static and dynamic masks and (ii) applying a threshold to retain only high-probability pixels. b) Object tracking as a filter to deal with partly immersed objects and to distinguish between moving objects from static waves.

736
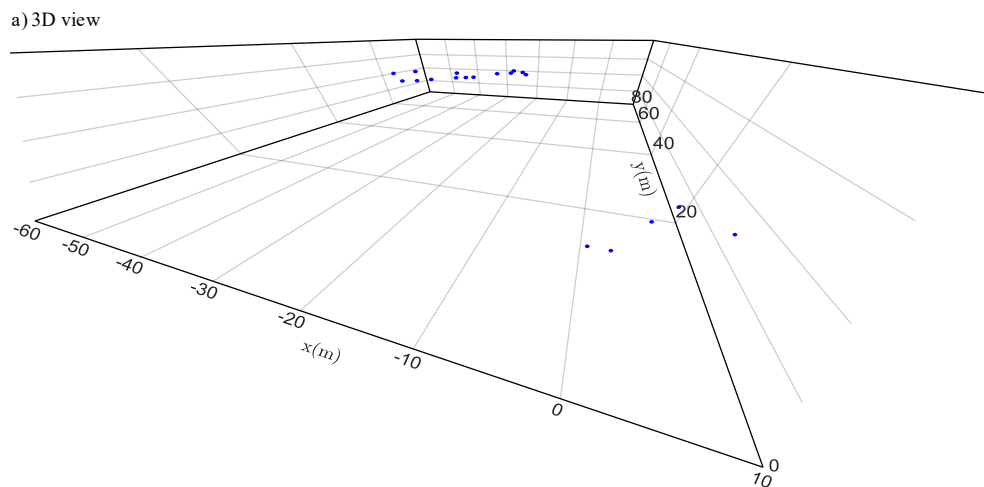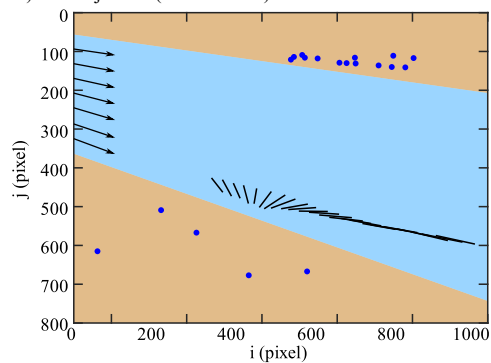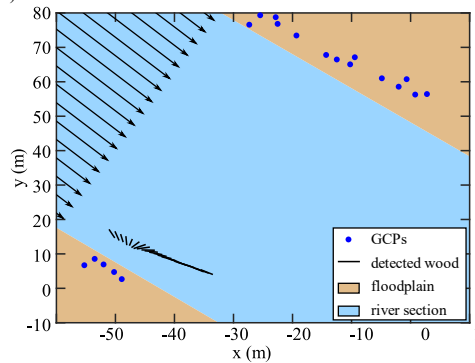
Fig 5 Image rectification, process. 3D view of non-colinear GCPs in metric coordinates (a), their corresponding localization within the image (b), and the relative 2D metric coordinates for a given water level (c). (b,c) A practical example of the transformation of the coordinates is presented. The different solid lines represent the successive detection in a set of consecutive frames.

737

Earth **Surface**
Dynamics
Discussions

738

Fig 6 User interface of the detection software.

739
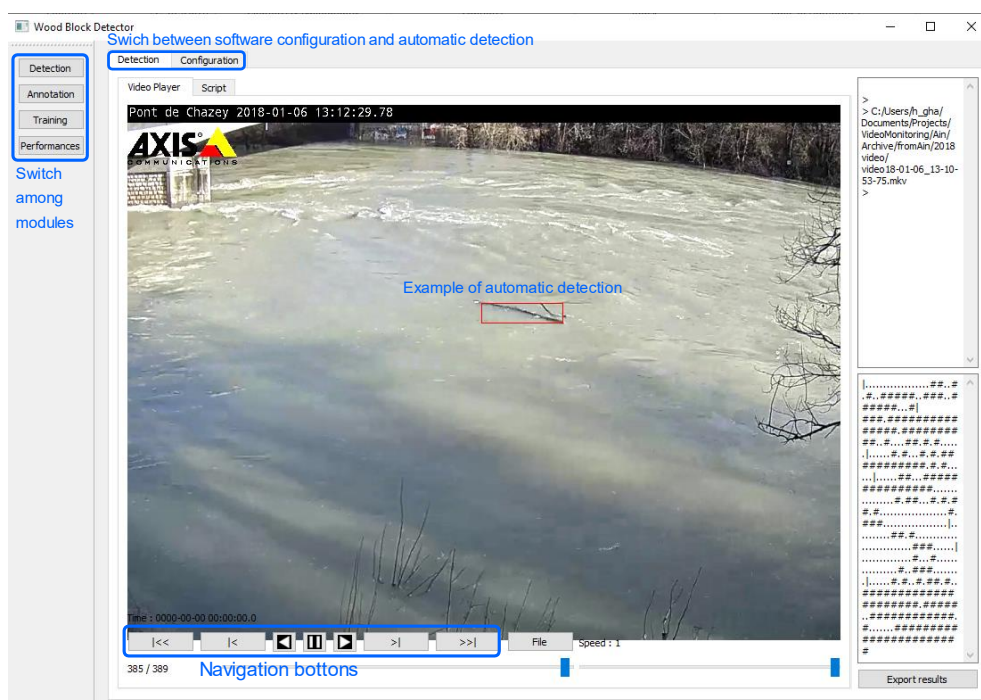
Fig 7 User interface of the detection module of automatic detection software.
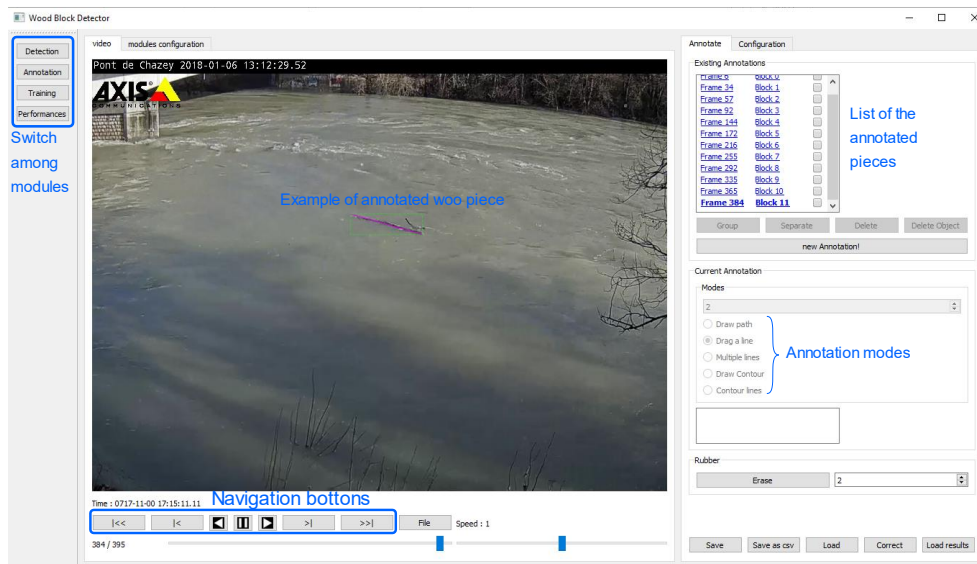
740

Fig 8 User interface of the annotation module of automatic detection software.
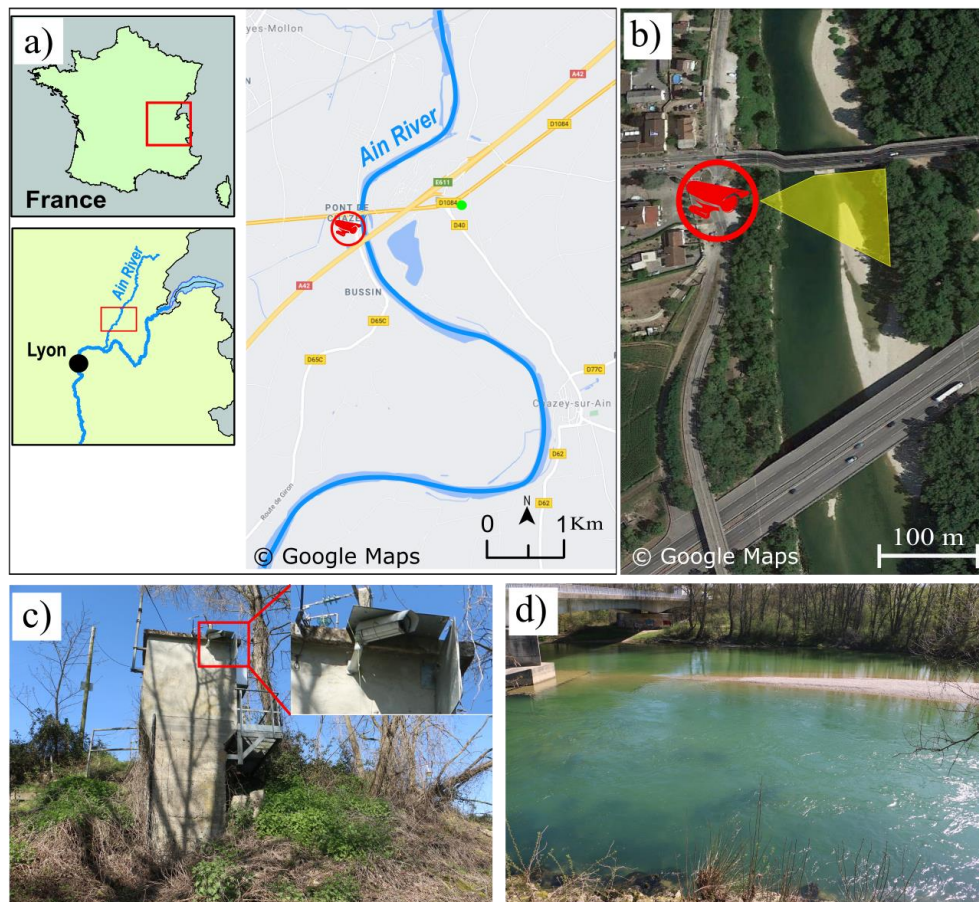
741

Fig 9 Study site at Pont de Chazey: a) Location of the Ain River catchment in France and location of the gauging and meteorological stations, b) camera position and its view angle in yellow, c) overview of the gauging station with the camera installation point.
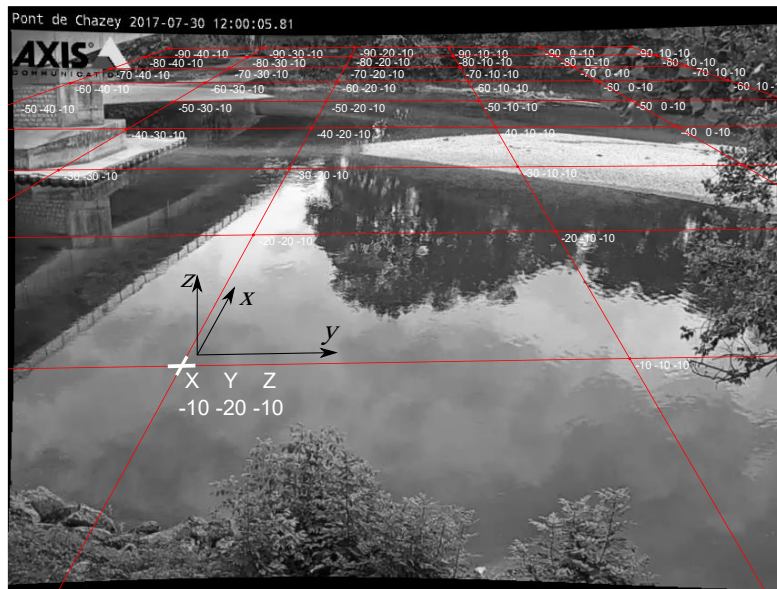
Fig 10 Rectifying transformation matrix at low flow level with camera at (0,0,0).
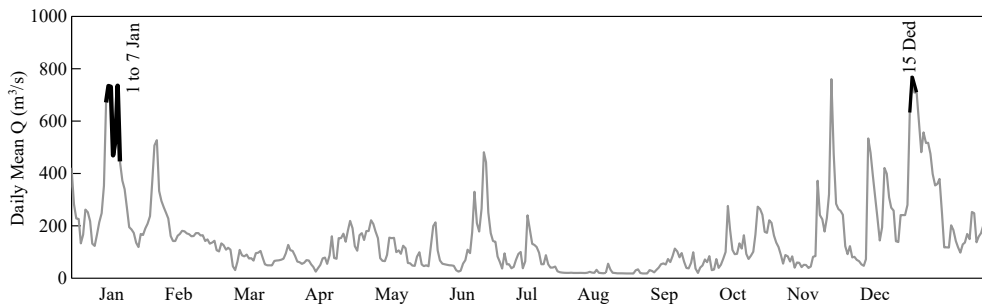
Fig 11 Daily mean discharge series for monitoring period from 1st to 7th January and in 15th December.

36

744

Fig 12 Different light conditions during (a) morning, (b) noon and (c) late afternoon, results in different frame roughness's and different detection performances.
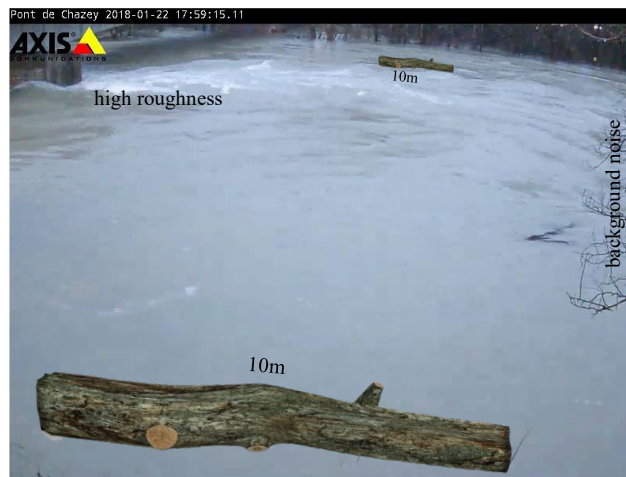
745

Fig 13 Wood position can highly affect the quality of detection. Pieces that are passing in front of the camera are detected much better than the pieces far from the camera.
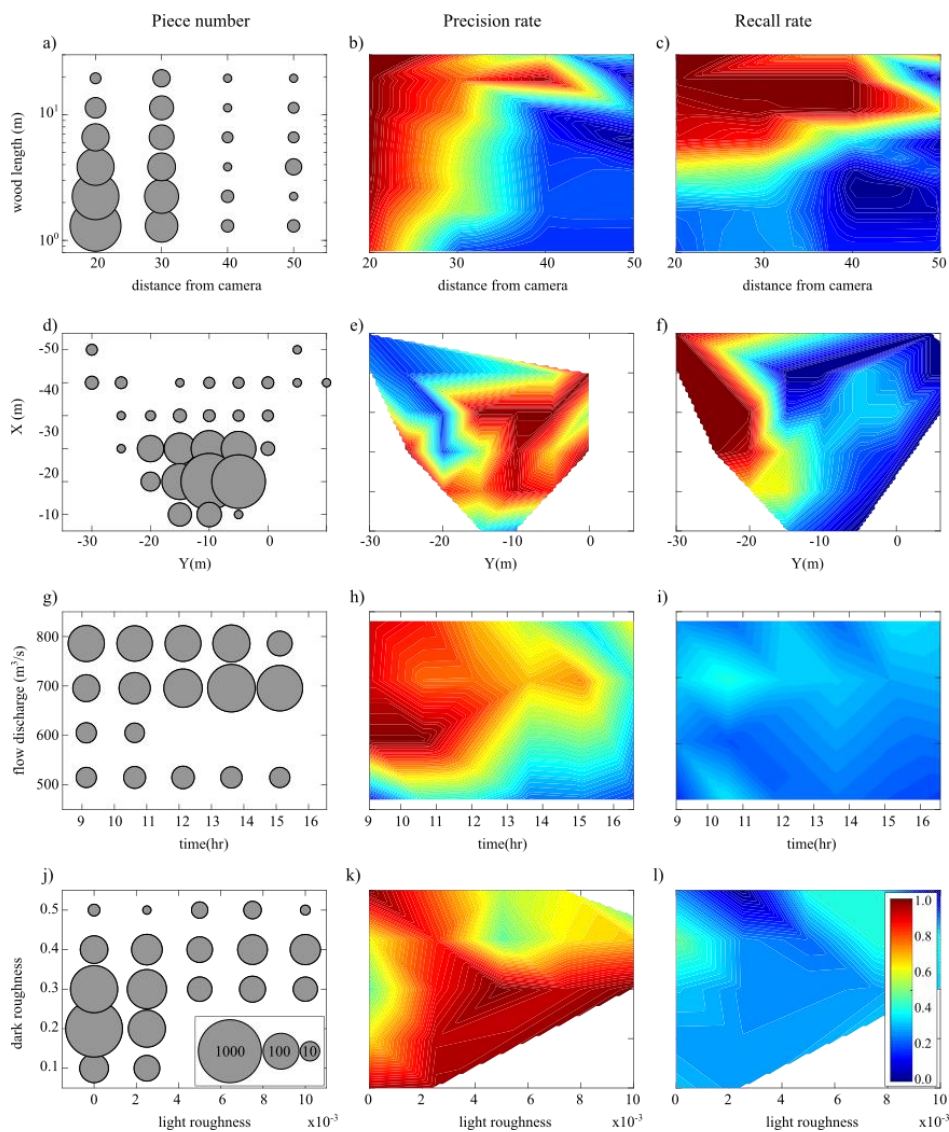
746

Fig 14 Correction matrices: a, b, c) wood lengths as a function of the distance from the camera, d, e, f) detection position, g, h, i) flow discharges during the daytime, and j, k, l) light and dark roughness's. The first column shows number of all annotated pieces. Second and third columns show Precision and Recall rates of the software respectively.

38
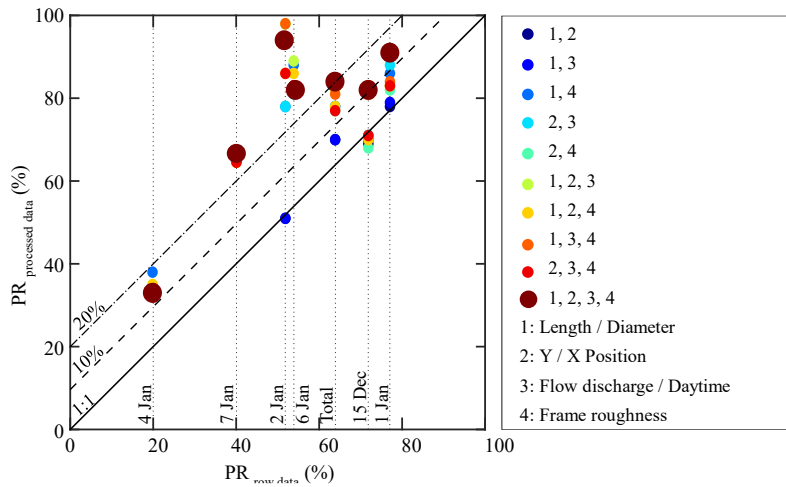
Fig 15 Effect of using different combinations of *PR* matrices on precision improvement compared with 1:1 line(no improvement), 10% and 20% improvement lines.

747
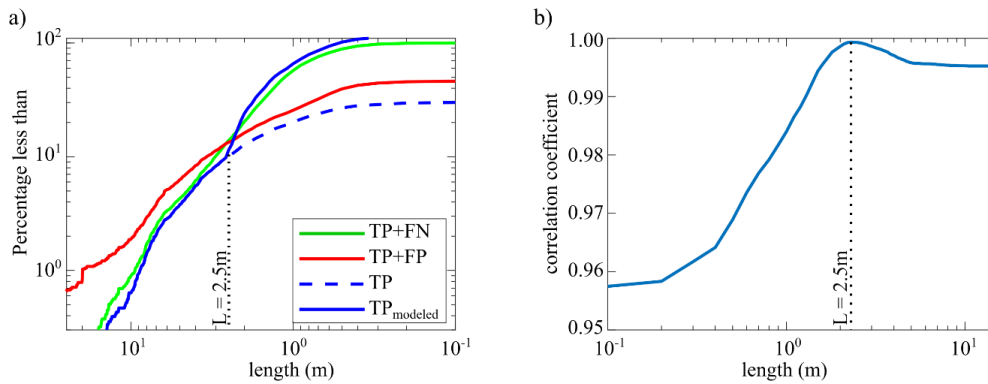
748

Fig 16 a) Steps to post-process software automatic detections: (i) raw detections (*TP + FP* red line), (ii) Only true positives using the *PR* improvement process (*TP* blue dashed line), and (iii) modeling false negatives (blue line). Operator annotation (green line is used as a benchmark). b) The correlation coefficient between operator annotation and modeled *TP* to find an optimum threshold length for *RR* improvement.

39
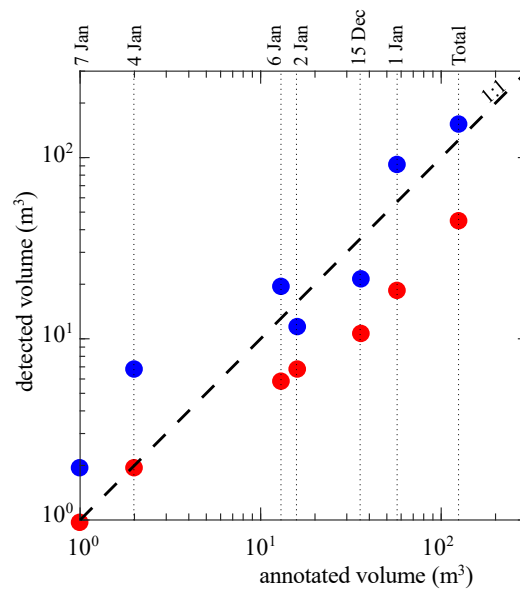
749

Fig 17 Comparison of the total volume of wood between operator annotation as the benchmark and raw data (red scatters) and post-processed data (blue scatters), compared with a 1:1 line.